

## FOREGROUND ANALYSIS FROM THE 1-YEAR WILKINSON MICROWAVE ANISOTROPY PROBE (WMAP) DATA

PAVEL D. NASELSKY<sup>1,2</sup>, OLEG V. VERKHODANOV<sup>3</sup>, LUNG-YIH CHIANG<sup>1</sup>, IGOR D. NOVIKOV<sup>1,4</sup>  
naselsky@nbi.dk

*Subject headings:* cosmology: cosmic microwave background — cosmology: observations — methods: data analysis

*Submitted to The Astrophysical Journal*

### ABSTRACT

We present a detailed analysis on the phases of the *WMAP* foregrounds (synchrotron, free-free and dust emission) of the *WMAP* K-W bands in order to estimate the significance of the variation of the spectral indices at different components. We first extract the spectral-index varying signals by assuming that the invariant part among different frequency bands have 100% cross-correlation of phases. We then use the minimization of variance, which is normally used for extracting the CMB signals, to extract the frequency independent signals. Such a common signal in each foreground component could play a significant role for any kind of component separation methods, because the methods cannot discriminate frequency independent foregrounds and CMB.

### 1. INTRODUCTION

The release of the first year data from the Wilkinson Microwave Anisotropy Probe (*WMAP*) provides a unique opportunity to investigate the properties of whole-sky cosmic microwave background (CMB) anisotropies at unprecedented resolution and sensitivity to date (Bennett et al. 2003b; Hinshaw et al. 2003a,b). The *WMAP* science team also produce several whole sky foreground maps of synchrotron, free-free and dust emission from all the frequency bands at the range 23-94 GHz with unprecedented precision (Bennett et al. 2003c). The analysis of the foreground properties is important as it is an indirect testing of the derived CMB signal properties (the angular power spectrum and its corresponding optimal values of the cosmological parameters for the best fit  $\Lambda$ CDM model (Tegmark, de Oliveira-Costa & Hamilton 2003; de Oliveira-Costa, Tegmark, Zaldarriaga & Hamilton 2003; Efstathiou 2003), and it also sheds light on the statistical properties of the CMB signal, i.e. Gaussianity of the CMB anisotropies (Komatsu et al. 2003; Chiang et al. 2003; Park 2004; Naselsky, Doroshkevich & Verkhodanov 2003, 2004; Eriksen et al. 2004a,b; Hansen et al. 2004).

In the framework of inflation paradigm, the angular power spectrum  $C_\ell$  provides *all* the information about the CMB fluctuations when the anisotropies constitute a Gaussian random field (Bardeen et al. 1986; Bond & Efstathiou 1987). Therefore, non-Gaussianity, either with primordial origin, or residuals from systematics or foreground component separation, shall inflict the accuracy of the cosmological parameters. Recently there are reports on detection of non-Gaussianity from 1-year derived CMB maps, which is attributed to foreground residuals or the systematic effect correction (Chiang et al. 2003; Naselsky, Doroshkevich & Verkhodanov 2003, 2004; Eriksen et al. 2004b; Hansen et al. 2004). This issue therefore needs to

be dealt with care before we reach any conclusions on, among other important issues, the statistical properties of the CMB anisotropies.

The *WMAP* science team use Maximum Entropy Method to produce five maps at K-W bands for the synchrotron component, five maps for the free-free emission. They also incorporate extrapolation of the galactic dust emission from 100 microns (Finkbeiner, Davis and Schlegel 1999) to *WMAP* frequency range. In this paper we examine the properties of the *WMAP* derived foreground maps, using an approach based on the phase of spherical harmonic coefficients. From theoretical point of view, the phases of the major foreground components listed above are extremely important. They provide an opportunity to develop and to implement so called “blind” method of the CMB and foregrounds separation not for the *WMAP* data only, but for the upcoming high-resolution PLANCK data as well.

The CMB and the combined foreground signals: synchrotron, free-free, dust emission and so on come from the same data sets. For the method by the *WMAP* science team for the CMB signal extraction, that by Tegmark, de Oliveira-Costa & Hamilton (2003) (TOH hereafter), Naselsky et al. (2003), and by Eriksen et al. (2004b), pronounced correlations of phases (hence correlations in morphology) between different frequencies at each foreground component are necessary (Tegmark & Efstathiou 1996; Bouchet & Gispert 1999; Hobson et al. 1998; Stolyarov et al. 2002; Delabrouille, Patanchon & Audit 2003; Tegmark, de Oliveira-Costa & Hamilton 2003; Patanchon et al. 2003; Barreiro et al. 2003; Martinez-Gonzalez et al. 2003), i.e. the foregrounds at different frequencies should only differ by amplitudes not by morphology. Using the derived maps for the synchrotron, free-free and dust emission from the

<sup>1</sup> Niels Bohr Institute, Blegdamsvej 17, DK-2100 Copenhagen, Denmark

<sup>2</sup> Rostov State University, Space Research Department, Zorge,5, 344091, Russia

<sup>3</sup> Special Astrophysical Observatory, Nizhnij Arkhyz, Karachaj-Cherkesia, 369167, Russia

<sup>4</sup> Astro Space Center of Lebedev Physical Institute, Profsoyuznaya 84/32, Moscow, Russia

WMAP web site <sup>5</sup> we demonstrate such correlations (see Section 1). Not surprisingly, these phases are not strongly correlated, especially for the synchrotron emission. Such deviation in morphology is mentioned by WMAP science team as the so-called spectral index variation effect (Bennett et al. 2003c). The aim of this paper is to find the foreground components of signal from K-W band which cause deviations in morphology in the foregrounds (Section 2 and 3) and some components which do not have any frequency dependence (Section 4). The latter creates some problems for the standard tools for CMB component separation and determines the corresponding error of the tools. Below we will mainly discuss the synchrotron, free-free and dust components, but our method can be easily expanded on all kind of foregrounds, which are important for the component separation tools for the *Planck* mission.

This paper is arranged as follows: in Section 2 we use phase analysis to develop a method for the spectral-index varying signals in the foreground maps. For the WMAP foreground maps the derived spectral-index varying signals are shown in Section 3. And in Section 4 we apply the minimization of the variance on the WMAP foreground maps to extract the frequency independent signals for each foreground component. We use circular statistics to test the cross correlations of those maps in Section 5. Conclusions and discussions are in Section 6.

## 2. SEPARATION OF THE SPECTRAL-INDEX VARYING SIGNAL IN THE WMAP FOREGROUND MAPS

We formulate the question as follows: how can we extract the common phases for each kind of the foregrounds from the WMAP derived foreground maps?

For that purpose we will apply circular phase statistics (Fisher 1993), using Lagrangian weighting coefficients  $w_j(\ell)$ , ( $\sum_j w_j(\ell) = \mathbf{I}$ ), similar to the TE96 optimization (Tegmark & Efstathiou 1996; Tegmark, de Oliveira-Costa & Hamilton 2003), but for the phases at each band  $j$ . For statistical characterization of the temperature fluctuations on a sphere we express each foreground signal as a sum over spherical harmonics

$$\Delta T(\theta, \varphi) = \sum_{\ell=0}^{\infty} \sum_{m=-\ell}^{\ell} |a_{\ell m}| e^{i\phi_{\ell m}} Y_{\ell m}(\theta, \varphi), \quad (1)$$

where  $|a_{\ell m}|$  and  $\phi_{\ell m}$  are the moduli and phases of the coefficients of the expansion.

In practice, we use the HEALPIX package (Górski, Hivon & Wandelt 1999) to decompose each of the WMAP foreground maps at K-W bands for the spherical harmonic coefficients  $a_{\ell m}$ . Then we take the *whitened* foreground maps for each frequency band  $j$ :

$$M_{\ell m}^{(j)} = \frac{a_{\ell m}}{|a_{\ell m}|} = \exp\left(i\Phi_{\ell m}^{(j)}\right), \quad (2)$$

and using the weighting coefficients  $w_j(\ell)$  on the phases we have the map, for example for the synchrotron emission  $\mathcal{S}_{\ell m}$ :

$$\begin{aligned} \mathcal{S}_{\ell m} &\equiv \exp\left(i\Phi_{\ell m}^{\mathcal{S}}\right) \\ &= \prod_{j=1}^N \left(M_{\ell m}^{(j),\mathcal{S}}\right)^{w_j(\ell)} = \exp\left(i \sum_j w_j(\ell) \Phi_{\ell m}^{(j),\mathcal{S}}\right). \end{aligned} \quad (3)$$

The weighting coefficients are designed to produce the map whose phases  $\Phi_{\ell m}^{\mathcal{S}} = \sum_j w_j(\ell) \Phi_{\ell m}^{(j),\mathcal{S}}$  do not depend on frequency. The map  $\mathcal{S}_{\ell m}$  represents the common part of the foregrounds (in morphology) among the K-W bands. Note that we can reach different sets of weighting coefficients for the maps of the free-free ( $\mathcal{F}_{\ell m}$ ) and the dust ( $\mathcal{D}_{\ell m}$ ) emissions.

### 2.1. Determination of the weighting coefficients

To obtain the weighting coefficients  $w_j(\ell)$  it is natural to assume that  $\Phi_{\ell m}^{\mathcal{S}}$  is orthogonal to the phase differences  $D_{\ell m}^{(i),\mathcal{S}} = \Phi_{\ell m}^{(i),\mathcal{S}} - \Phi_{\ell m}^{(5),\mathcal{S}}$ ,  $i = 1 - 5$  corresponds to the K, Ka, Q, V and W bands, respectively. Taking into account of  $\sum_j w_j(\ell) = \mathbf{I}$  in Eq.(3) we have (for generality we drop the superscript  $\mathcal{S}$ )

$$\Phi_{\ell m} = \Phi_{\ell m}^{(5)} + \sum_{j=1}^4 w_j(\ell) D_{\ell m}^{(j)} \quad (4)$$

where  $D_{\ell m}^{(j)} = \Phi_{\ell m}^{(j)} - \Phi_{\ell m}^{(5)}$ . The orthogonality of  $\Phi_{\ell m}$  and  $D_{\ell m}^{(j)}$  leads to

$$\sum_{m=1}^{\ell} \Phi_{\ell m} D_{\ell m}^{(j)} = 0 \quad j = 1, 2, 3, 4 \quad (5)$$

However, considering  $2\pi$  periodicity of the phases, a simple generalization of Eq.(5) should be considered, which can be obtained by the following way (Fisher 1993). We introduce the trigonometric variables

$$x_{\ell m} = \sin \Phi_{\ell m}; \quad y_{\ell m}^{(j)} = \sin D_{\ell m}^{(j)} \quad (6)$$

and the cross-correlation coefficients  $r$  defined as follows should produce zero value due to orthogonality, i.e.

$$r(\ell) = \sum_{m=1}^{\ell} \sin \Phi_{\ell m} \sin D_{\ell m}^{(k)} \equiv 0. \quad (7)$$

As one can see from Eq.(7), if the phase difference  $D_{\ell m}^{(k)}$  and  $\Phi_{\ell m}$  are small ( $\ll \pi/2$ ), we will have the same equation for the weighting coefficients as Eq.(5). If  $D_{\ell m}^{(k)}$  is small, but  $\Phi_{\ell m}$  is comparable with  $\pi/2$  we will have non-linear equation for the weighting coefficients that can be solved numerically.

### 2.2. Spectral-index varying foregrounds

We now can derive, from the given coefficients  $\mathbf{w}$ , the maps for each component of the foregrounds (synchrotron, free-free and dust emission) with the common phases of components among all frequency bands as follows:

$$\begin{aligned} a_{\ell m}^{(j),\mathcal{S},\mathcal{F},\mathcal{D}} &= \left| a_{\ell m}^{(j),\mathcal{S},\mathcal{F},\mathcal{D}} \right| \exp\left(i\Phi_{\ell m}^{\mathcal{S},\mathcal{F},\mathcal{D}}\right) \\ &= \left| a_{\ell m}^{(j),\mathcal{S},\mathcal{F},\mathcal{D}} \right| \exp\left(i \sum_j w_j(\ell) \Phi_{\ell m}^{(j),\mathcal{S},\mathcal{F},\mathcal{D}}\right), \end{aligned} \quad (8)$$

where  $j$  denotes the frequency bands,  $\mathcal{S}$ ,  $\mathcal{F}$ ,  $\mathcal{D}$  denote the synchrotron, free-free and dust emission, respectively, and  $\Phi_{\ell m}^{(j)}$  corresponds to each component at each band. The

<sup>5</sup> [http://lambda.gsfc.nasa.gov/product/map/m\\_products.cfm](http://lambda.gsfc.nasa.gov/product/map/m_products.cfm)

maps of spectral-index varying signal at each band for each foreground component are

$$a_{\ell m}^{(j),S,\mathcal{F},\mathcal{D}} = \left| a_{\ell m}^{(j),S,\mathcal{F},\mathcal{D}} \right| \left[ \exp \left( i \Phi_{\ell m}^{(j),S,\mathcal{F},\mathcal{D}} \right) - \exp \left( i \sum_j w_j(\ell) \Phi_{\ell m}^{(j),S,\mathcal{F},\mathcal{D}} \right) \right] \quad (9)$$

Taking into account Eq.(9) one gets the map of fluctuation

$$a_{\ell m}^{(j),S,\mathcal{F},\mathcal{D}} \simeq \left| a_{\ell m}^{(j),S,\mathcal{F},\mathcal{D}} \right| \Delta_{\ell m}^{(j)} \exp \left[ i \left( \Phi_{\ell m}^{(j),S,\mathcal{F},\mathcal{D}} + \frac{\pi}{2} \right) \right], \quad (10)$$

where  $\Delta_{\ell m}^{(j)} = \Phi_{\ell m}^{(j)} - \Phi_{\ell m}$ . The map from Eq.(10) represents all variation of the phase for all  $m \geq 1$  harmonics of the signal, if  $\Delta_{\ell m}^{(j)} \ll 1$ . As one can see, for that map the moduli are  $|a_{\ell m}^{(j),S,\mathcal{F},\mathcal{D}}| |\Delta_{\ell m}^{(j)}|$  and the phases are the initial phases rotated by the angle  $\pi/2$ , if  $\Delta_{\ell m}^{(j)} > 0$  and by the angle  $3\pi/2$ , if  $\Delta_{\ell m}^{(j)} < 0$ .

### 3. THE SPECTRAL-INDEX VARYING SIGNALS IN THE WMAP SYNCHROTRON, FREE-FREE AND DUST MAPS

We implement the method we have developed to extract the peculiar signals for the synchrotron, free-free and dust emission for the *WMAP* frequency bands. We do not include the K band in our analysis due to the same reason as the *WMAP* science team mentions. The maps for the spectral-index varying signals are grouped in three: synchrotron, free-free and dust emission.

In Fig.1 we plot the maps for the spectral-index varying signal of the synchrotron emission for the *WMAP* Ka-W bands. The  $m = 0$  modes in these spectral-index varying maps have zero amplitude. It is the reason why synchrotron maps looks peculiar.

Fig.2 and 3 are the spectral-index varying signals for the free-free and dust emission, respectively. Again the  $m = 0$  modes are naturally excluded.

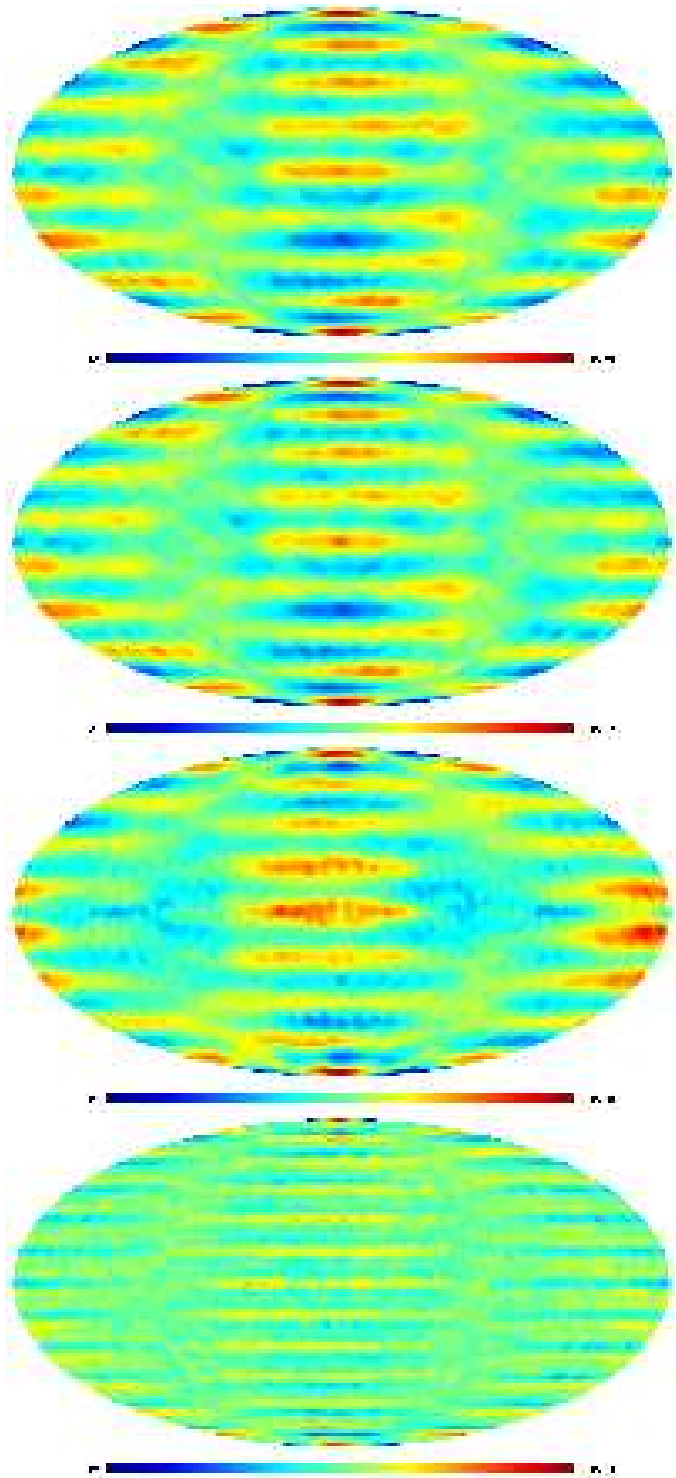


FIG. 1.— The derived spectral-index varying signals for the synchrotron component. From top to bottom are Ka, Q, V and W bands.

For the *WMAP* dust maps the spectral-index varying signals are relatively weak in comparison with those from the synchrotron and free-free maps. However, it is in order of 30% of the amplitude of ILC signal which should be taken into account seriously.

In Fig.4 we display the spectral-index varying signals, the sum of the synchrotron, free-free and dust emission.

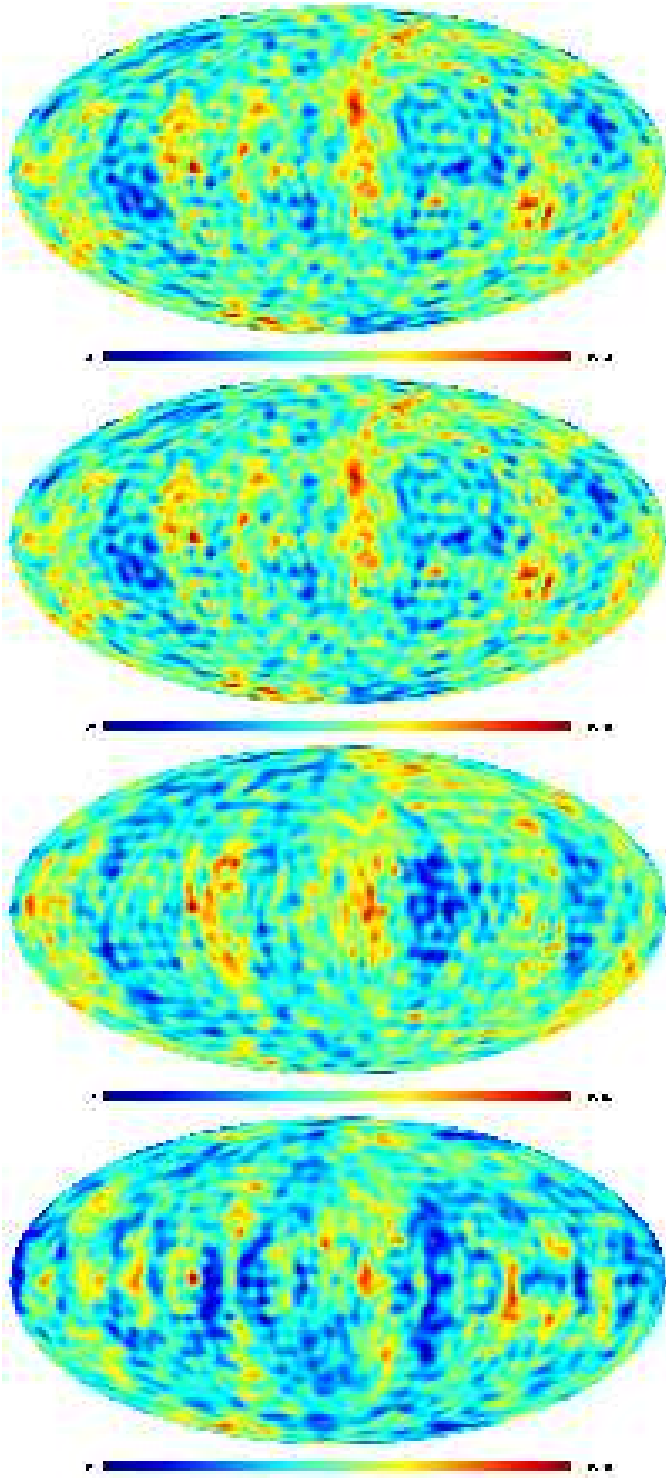


FIG. 2.— The derived spectral-index varying signals for the free-free emission. From top to bottom are Ka, Q, V and W bands.

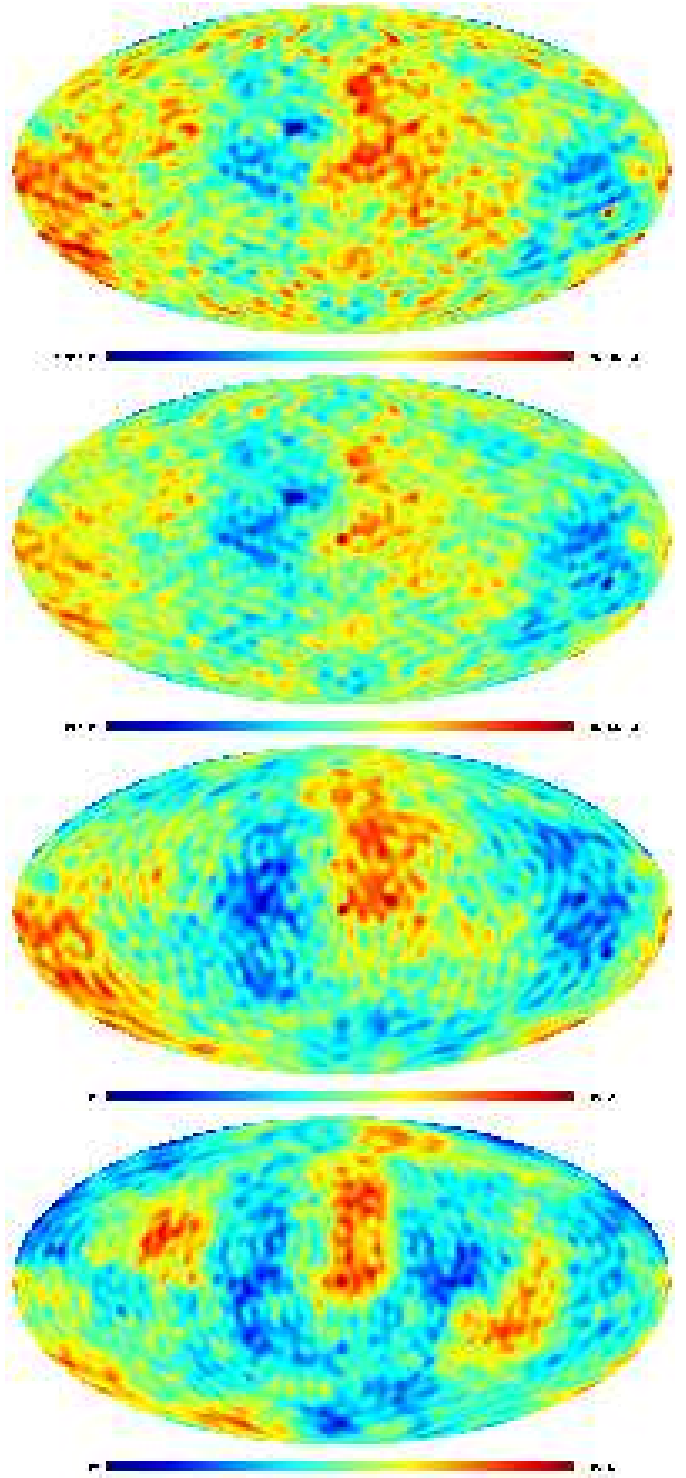


FIG. 3.— The derived spectral-index varying signals for the dust emission. From top to bottom are Ka, Q, V and W bands.

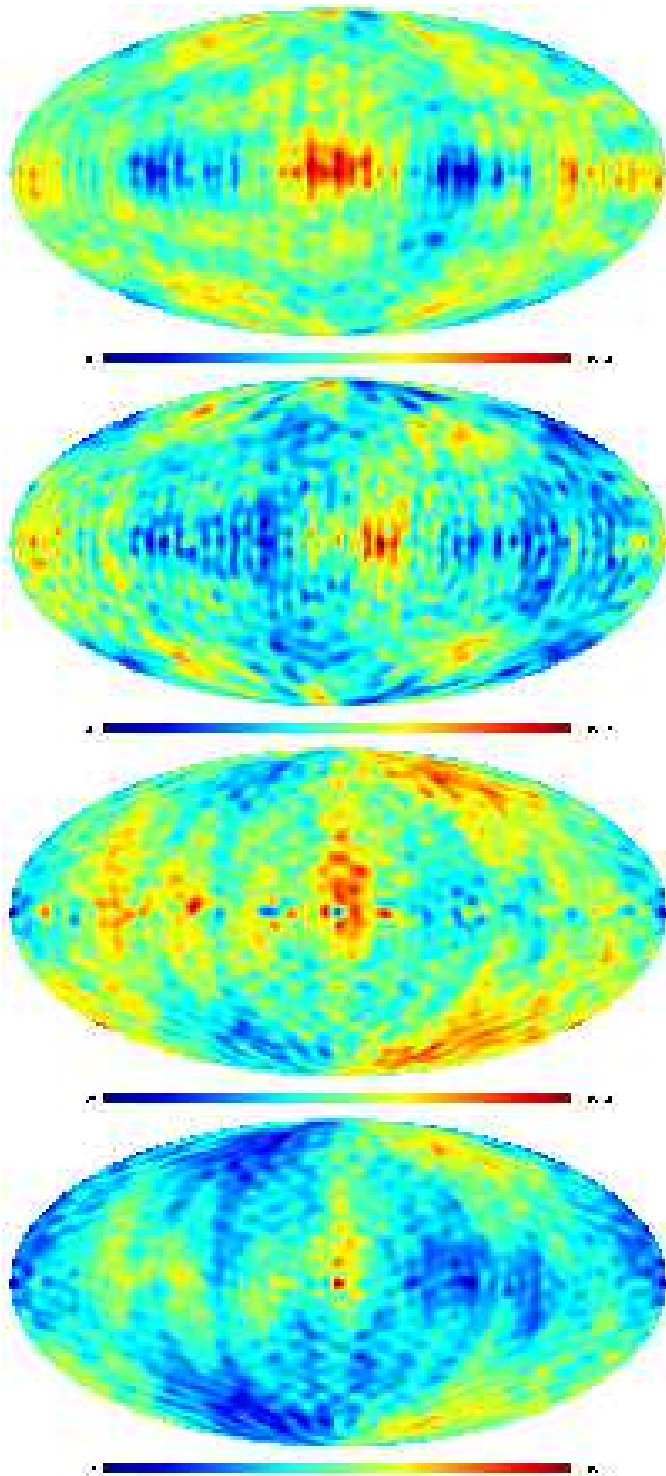


FIG. 4.— The derived spectral-index varying signals of the sum of the synchrotron, free-free and dust emissions. From top to bottom are ka, Q, V and W bands.

#### 4. THE FREQUENCY INDEPENDENT SIGNALS (FIS) IN THE WMAP FOREGROUND MAPS

In this Section we use the minimization of the variance in a similar fashion on the WMAP foreground maps for the frequency independent signals (hereafter FIS). This method is mainly used by the WMAP science team to produce the CMB map (Bennett et al. 2003c) using a weighted combination of the 5 bands outside the Galactic plane.

Tegmark, de Oliveira-Costa & Hamilton (2003) (hereafter TOH) perform an independent foreground analysis from the WMAP data using weighting coefficients dependent not only on the angular scales ( $\ell$ ) but also on the Galactic latitudes. Below we use the TOH method for the synchrotron, free-free and dust maps in order to extract the frequency independent component (or partly independent for some of the frequency range) without any assumptions about the statistical nature of the derived signals. Moreover, we use the whole sky for analyses and do not apply any Galaxy plane cut-off and masks, nor do we dissect the whole sky into disjoint regions.

Using minimization scheme by TOH and Tegmark & Efstathiou (1996), we implement the blind method for the FIS for synchrotron, free-free and dust emission which have the same phases for K-W bands. Unlike Section 1, here we are looking for some common component of the foregrounds, which is frequency independent at the WMAP frequency range. Moreover, such a common component could play a significant role for any kind of component separation methods, because the methods cannot discriminate frequency independent foregrounds and CMB.

##### 4.1. The synchrotron FIS maps

We firstly group the maps in the following combinations for the WMAP synchrotron maps: Ka-Q, Ka-V and Q-V. For each pair of the maps (Ka-Q, Ka-V and Q-V) we want to reach the common Synchrotron emission map ( $a_{\ell m}^S \equiv \mathbf{S}$ ) which has the same phases for each pair of the bands and for each  $\ell, m$  mode. We use the optimization coefficients  $\Gamma^{(i)} \equiv \Gamma_{\ell}^{(i)}$ , similar to that by TE96 Tegmark & Efstathiou (1996), TOH, Naselsky et al. (2003):

$$\mathbf{S} = a_{\ell m}^S = \sum_{i=1}^2 \Gamma_{\ell}^{(i)} a_{\ell m}^{(i)} \equiv \sum_{i=1}^2 \Gamma^{(i)} \mathbf{a}^{(i)}, \quad (11)$$

where  $i = 1, 2$  correspond to the two bands in a pair. The  $\Gamma^{(i)}$  coefficients are subject to the following constraints

$$\frac{\delta \sum_{m=-\ell}^{\ell} |\mathbf{S}|^2}{\delta \Gamma^{(i)}} = 0, \quad (12)$$

and

$$\sum_i \Gamma^{(i)} = \mathbf{I}, \quad (13)$$

where  $\delta/\delta \Gamma^{(i)}$  denotes functional derivatives.

The  $\Gamma^{(i)}$  then have the following forms

$$\Gamma^{(1)} = \frac{\sum_{m=-\ell}^{\ell} \{ |\mathbf{a}^{(2)}| [ |\mathbf{a}^{(2)}| - |\mathbf{a}^{(1)}| \cos(\Psi^{(2)} - \Psi^{(1)}) ] \}}{\sum_{m=-\ell}^{\ell} |\mathbf{a}^{(1)} - \mathbf{a}^{(2)}|^2},$$

$$\Gamma^{(2)} = \frac{\sum_{m=-\ell}^{\ell} \{ |\mathbf{a}^{(1)}| [ |\mathbf{a}^{(1)}| - |\mathbf{a}^{(2)}| \cos(\Psi^{(2)} - \Psi^{(1)}) ] \}}{\sum_{m=-\ell}^{\ell} |\mathbf{a}^{(1)} - \mathbf{a}^{(2)}|^2}, \quad (14)$$

where  $\Psi^{(i)}$  are the phases of the synchrotron signal  $\mathbf{a}^{(i)}$  at the  $i$ -th map.

Then we obtain the common signal  $\mathbf{S}$  and the frequency dependent part  $F_{\ell m}^{(j)}$  at each  $j$ -th bands.

$$F_{\ell m}^{(1)} = \mathbf{a}^{(1)} - \mathbf{S} = \Gamma^{(2)} (\mathbf{a}^{(1)} - \mathbf{a}^{(2)})$$

$$F_{\ell m}^{(2)} = \mathbf{a}^{(2)} - \mathbf{S} = -\Gamma^{(1)} (\mathbf{a}^{(1)} - \mathbf{a}^{(2)}). \quad (15)$$

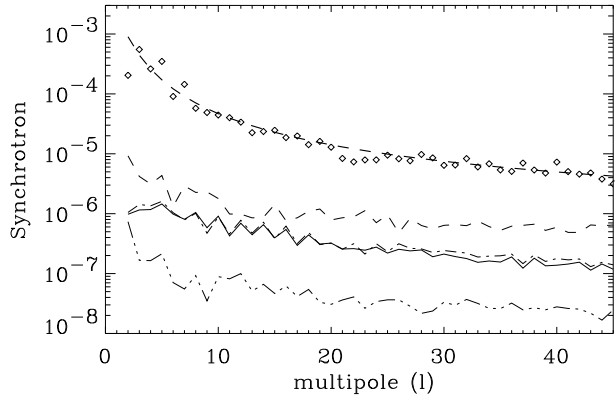


FIG. 5.— The power spectra of the common component from the synchrotron emission. Top thick dash line corresponds to the WMAP best fit  $\Lambda$ CDM model. Boxes reproduce the ILC power spectrum. Thin long dash line is the common component from Ka-Q synchrotron maps. Solid line is the common component from Ka-V synchrotron maps. Dash-dot line is that from Q-V and Dash dot-dot line is that from V-W. In Fig.5 we plot the power spectra for the FIS taken from different combinations of the WMAP synchrotron maps. As one can see, for Q-V bands and Ka-V bands we have the frequency independent component.

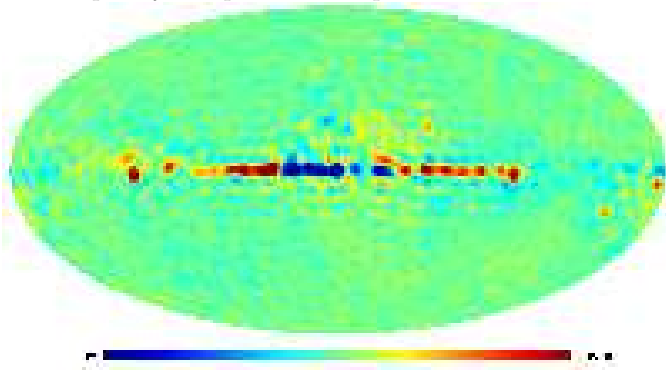


FIG. 6.— The FIS from Q-V synchrotron maps.

In Fig.6 we show the FIS from Q-V synchrotron maps, which mainly concentrated in the Galactic plane, but some of the point source residues seen above and below it. The power spectra of such FIS shown in Fig.5 is smaller than the ILC power, as shown in Fig.5. However, due to the source clustering in the Galactic plane it can significantly perturb the CMB map at Galactic plane region (see for example, Naselsky et al. (2003)).

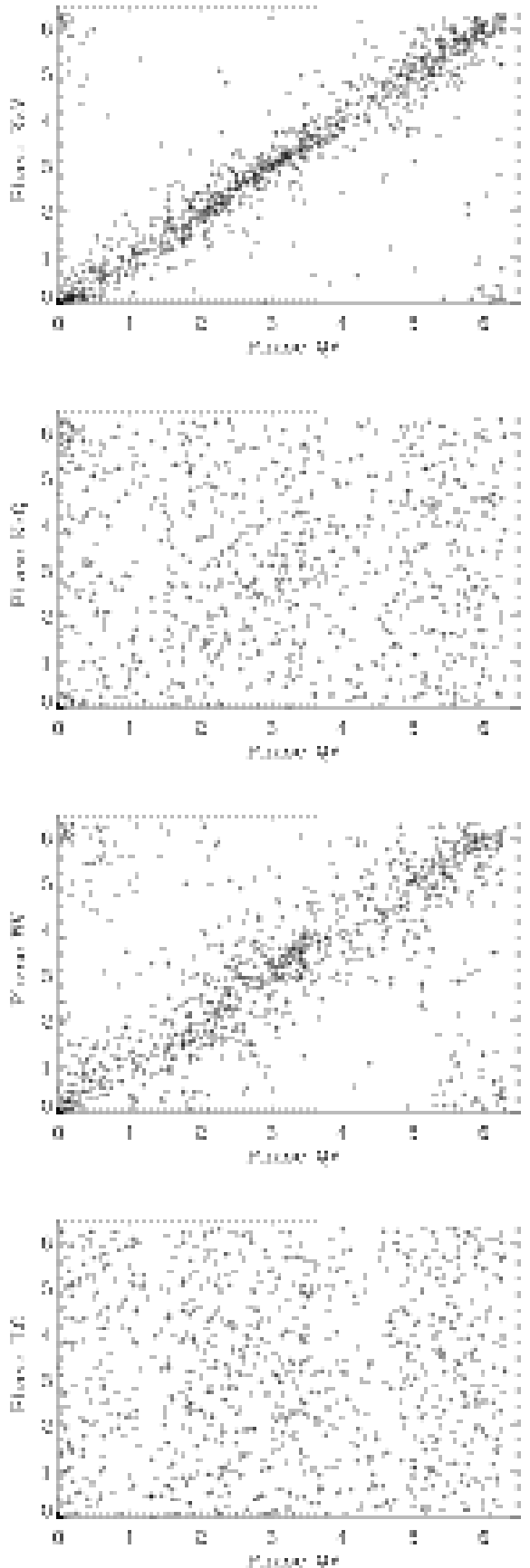


FIG. 7.— Reconstructed phases of the FIS from synchrotron maps with different combination of the bands. From top to bottom panels are cross-correlation between combination of Ka-V ( $y$ -axis) against Q-V ( $x$ -axis), Ka-Q against Q-V, V-W against Q-V, and ILC against Q-V.

In Fig.7 we plot the cross-correlations of phases for the synchrotron FIS obtained at different frequency bands. This Figure confirms that the FIS is common for Ka-V bands.

#### 4.2. The dust FIS maps

We show the dust FIS, using the same separation technique as for synchrotron emission.

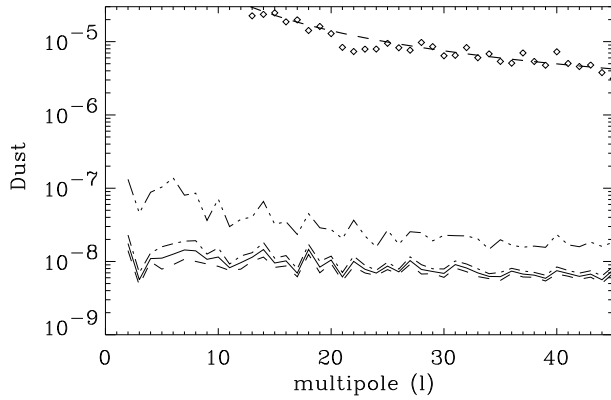


FIG. 8.— The power spectra of the common component from the dust emission. Top thick dash line corresponds to the *WMAP* best fit  $\Lambda$ CDM model. Boxes reproduce the ILC power spectrum. Thin long dash line is the common component from Ka-Q synchrotron maps. Solid line is the common component from Ka-V synchrotron maps. Dash-dot line is that from Q-V and Dash dot-dot line is that from V-W.

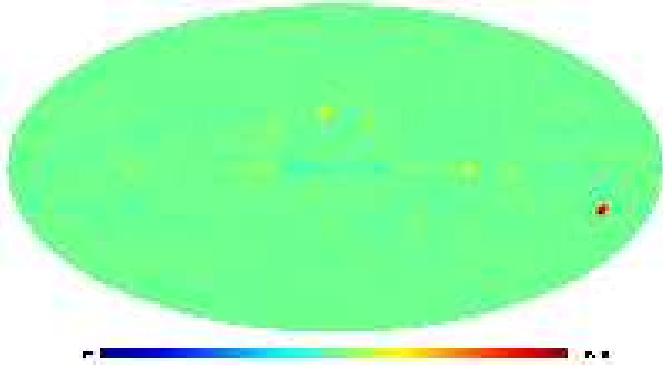


FIG. 9.— The FIS from Q-V dust maps.

Fig.8 is the power spectra. As shown in Fig.9 the FIS is mainly related to the point sources. Contamination of the Galactic plane signal is weak. In Fig.10 we plot the cross correlation of phases for the FIS at different combinations of the bands. These correlations are very strong for all Ka-V bands.

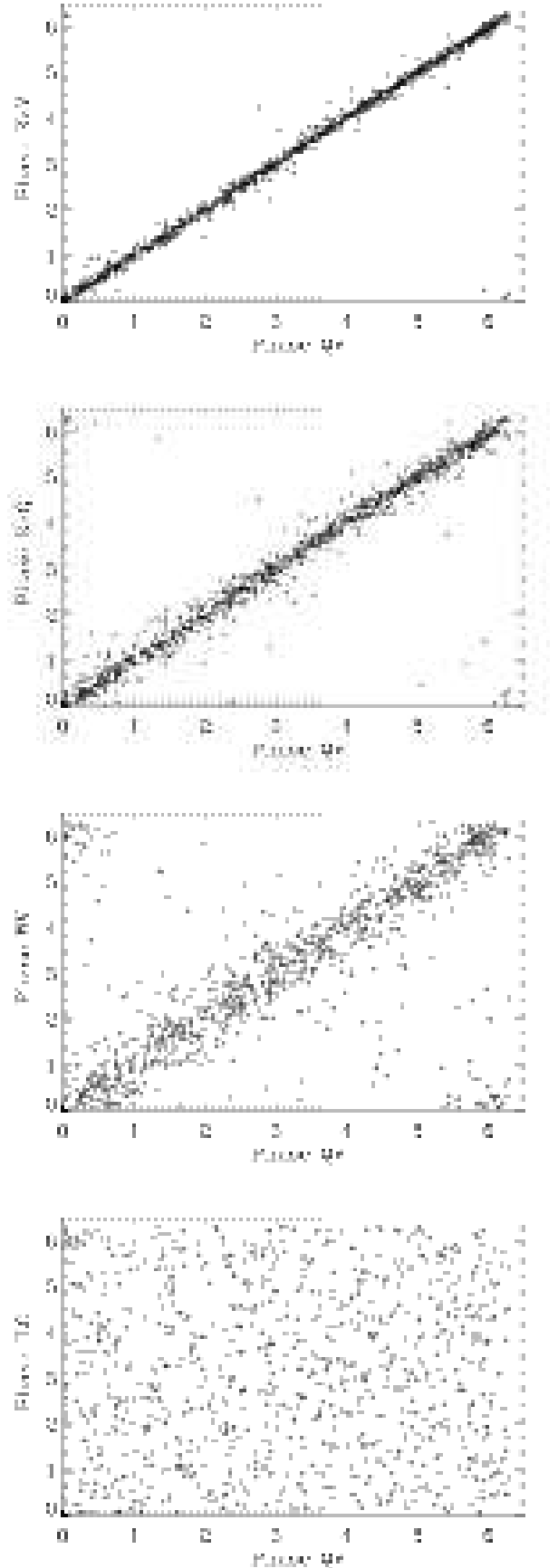


FIG. 10.— Reconstructed phases of the FIS from the dust maps with different combination of the bands. From top to bottom panels are cross-correlation between combination of Ka-V ( $y$ -axis) against Q-V ( $x$ -axis), Ka-Q against Q-V, V-W against Q-V, and ILC against Q-V.

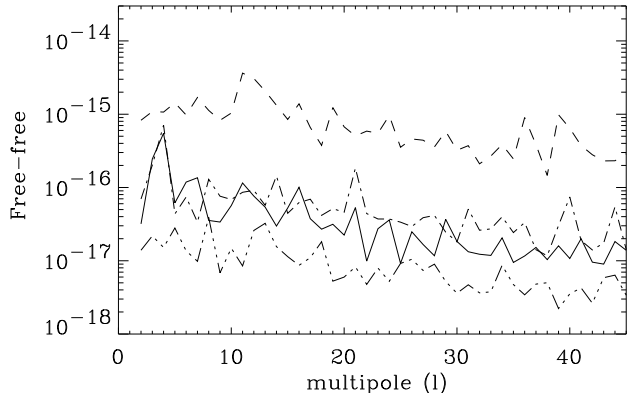


FIG. 11.— Power spectra for the common component from free-free emission. The definition of the lines are the same as in Fig.5. The power spectra are different for different frequency bands and phases of the signal are not highly correlated. Actually, the free-free component of the WMAP foreground is the only one which does not have FIS.

#### 4.3. The free-free FIS maps

For the free-free emission the derived FIS is extremely weak, as one can see from the Fig.11.

### 5. CROSS CORRELATION OF PHASES BETWEEN THE DERIVED CMB MAPS AND THE FOREGROUNDS

The aim of this Section is to show how the variation of the spectral index in the foreground components can manifest themselves in the CMB signal, which should be clean from the foreground contamination. We use the whole-sky maps derived from the WMAP data using different separation methods. Namely we use the WMAP Internal Linear Combination (ILC) map, the foreground cleaned map (FCM) and Wiener filtered map (WFM) by TOH, and the phase cleaned map (PCM) by Naselsky et al. (2003).

We use the trigonometric moment statistics to counter the circular nature of phases (Fisher (1993), see also Naselsky, Doroshkevich & Verkhodanov (2003)). We define the following trigonometric moments:

$$\begin{aligned} \mathbf{C}(\ell, \Delta\ell) &= \frac{1}{\ell - \ell'} \sum_{m=1}^{\ell - \ell'} \cos(\Phi_{\ell - \ell', m} - \Psi_{\ell + \ell'', m}); \\ \mathbf{S}(\ell, \Delta\ell) &= \frac{1}{\ell - \ell'} \sum_{m=1}^{\ell - \ell'} \sin(\Phi_{\ell - \ell', m} - \Psi_{\ell + \ell'', m}); \\ r^2(\ell, \Delta\ell) &= [\mathbf{C}^2(\ell, \Delta\ell) + \mathbf{S}^2(\ell, \Delta\ell)] \ell, \end{aligned} \quad (16)$$

where  $\Delta\ell = \ell' + \ell''$  and  $\Psi_{\ell m}$  are the phases of the foreground-cleaned signals (ILC, FCM, WFM, PCM) at each  $\ell m$  harmonic and  $\Phi_{\ell m}$  are the phases of the foregrounds. As we have shown, the most dangerous component of the foreground at each frequency band is the spectral index varying tail in the synchrotron, free-free and dust emission, shown in Fig. Below we plot the cross correlation function  $\mathbf{S}$ ,  $\mathbf{C}$  and  $r^2$  for each of the foreground cleaned signals. Using the statistics we look for signatures that deviate from the 68% CL. If the phases of the cleaned

map are highly correlated with those of the foregrounds, the  $\mathbf{C}$  statistic has asymptotics to unity, whereas the  $\mathbf{S}$  to zero. For the case of non-correlations, both  $\mathbf{C}$  and  $\mathbf{S}$  statistics have  $\ell^{1/2}$  asymptotics due to “random walk”.

In Fig.12 and 13 we plot the  $\mathbf{S}$ ,  $\mathbf{C}$  and  $r^2$  statistics on the foreground-cleaned and the foreground maps. The top 3 rows of Fig.12 is the statistics for ILC and foregrounds, in which from left to right columns are for  $\Delta\ell = 0, 1$  and 2, respectively. One can see significant cross correlations at multipoles  $\ell = 6, 8, 14-16, 21, 39$  and 47 of ILC with Q, V and W foregrounds at 95% CL and at  $\ell = 11, 17, 26, 36$  and 47 at 99% CL. The bottom 3 rows of Fig.12 is the statistics on PCM and the foregrounds. PCM is produced without galactic cut-off and any preliminary information about foreground properties (Naselsky et al. 2003). The possible non-Gaussianity in the PCM is the residues of bright point sources in the Galactic plane region covered by WMAP Kp2 mask. These residues have pronounced cross correlations with the synchrotron component as shown in Fig.6. In Fig.13 on the top 3 rows we can also see clearly some multipoles with cross correlations above  $2-\sigma$  and for  $\ell = 30$  the correlation is above 99% CL.

To show the possible multipole range in which contamination of non-Gaussian features can be important, in Fig.14 we plot the difference between the best-fit WMAP  $\Lambda$ CDM, ILC and TOH FCM power spectra, normalized to the  $\Lambda$ CDM power. The intriguing features appear at multipoles  $\ell = 2, 5, 7, 20 - 23, 40$ , in which the peaks of  $\Delta C_\ell / C_\ell$  lies above 68% CL.

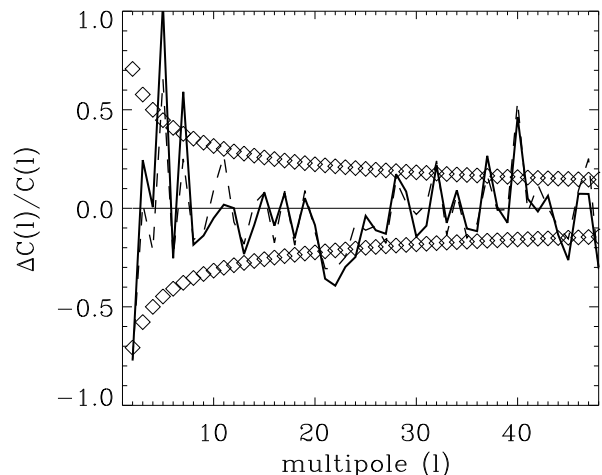


FIG. 14.— The difference between the best-fit WMAP  $\Lambda$ CDM, ILC and TOH FCM power spectra, normalized to the  $\Lambda$ CDM power. The diamond shape curves represent the cosmic variance.

### 6. CONCLUSIONS AND DISCUSSIONS

In this paper we raise the issue of how different the foreground maps at different frequency bands. From each WMAP foreground component: synchrotron, free-free and dust maps, we look for spectral-index varying signals. By assuming that the spectral-index *invariant* part has 100% phase correlation (hence the same morphology) among the different frequency bands, we develop a new method for extracting the spectral-index varying signals, which correspond to perturbations in phases. We have shown that this



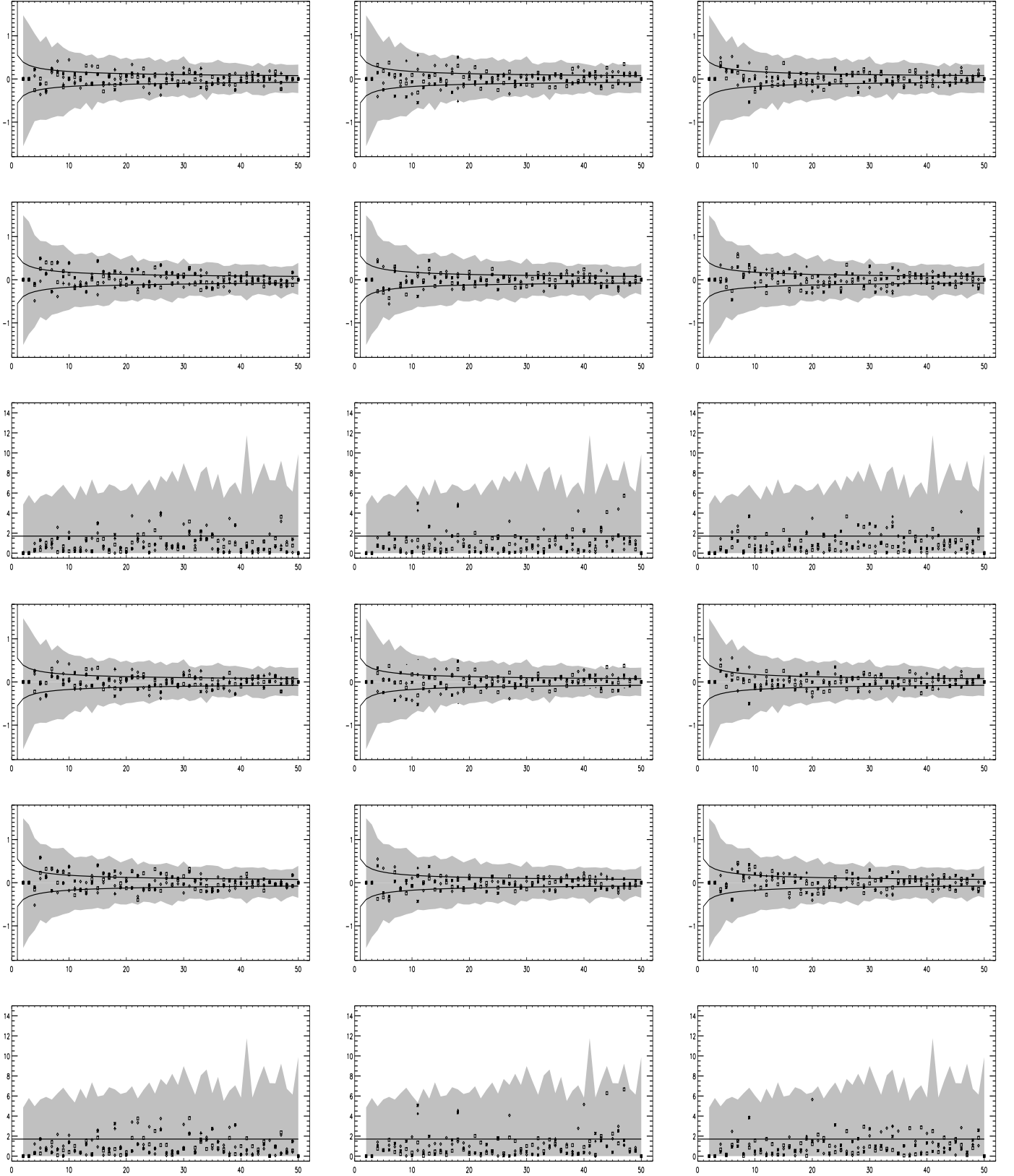


FIG. 12.— The circular statistics for the cross correlation of phases between the ILC and the foreground maps (top 3 rows) and between the PCM and the foreground maps (lower 3 rows). Each 3 rows (downwards) are **S**, **C** and  $r^2$  statistics, respectively. The 3 columns from left to right are for  $\Delta\ell = 0, 1$  and  $2$ , respectively. In each panel, the star sign marks ILC-Ka foreground cross correlation, the plus sign marks ILC-Q, the diamond sign marks ILC-V and the box sign ILC-W. The solid curves denote  $1-\sigma$  CL and the shaded areas cover 1000 Gaussian realizations from Monte Carlo simulations. The right column are **S**, **C** and  $r^2$  statistics between the PCM and foregrounds for  $\Delta\ell = 0, 1$  and  $2$ , respectively.

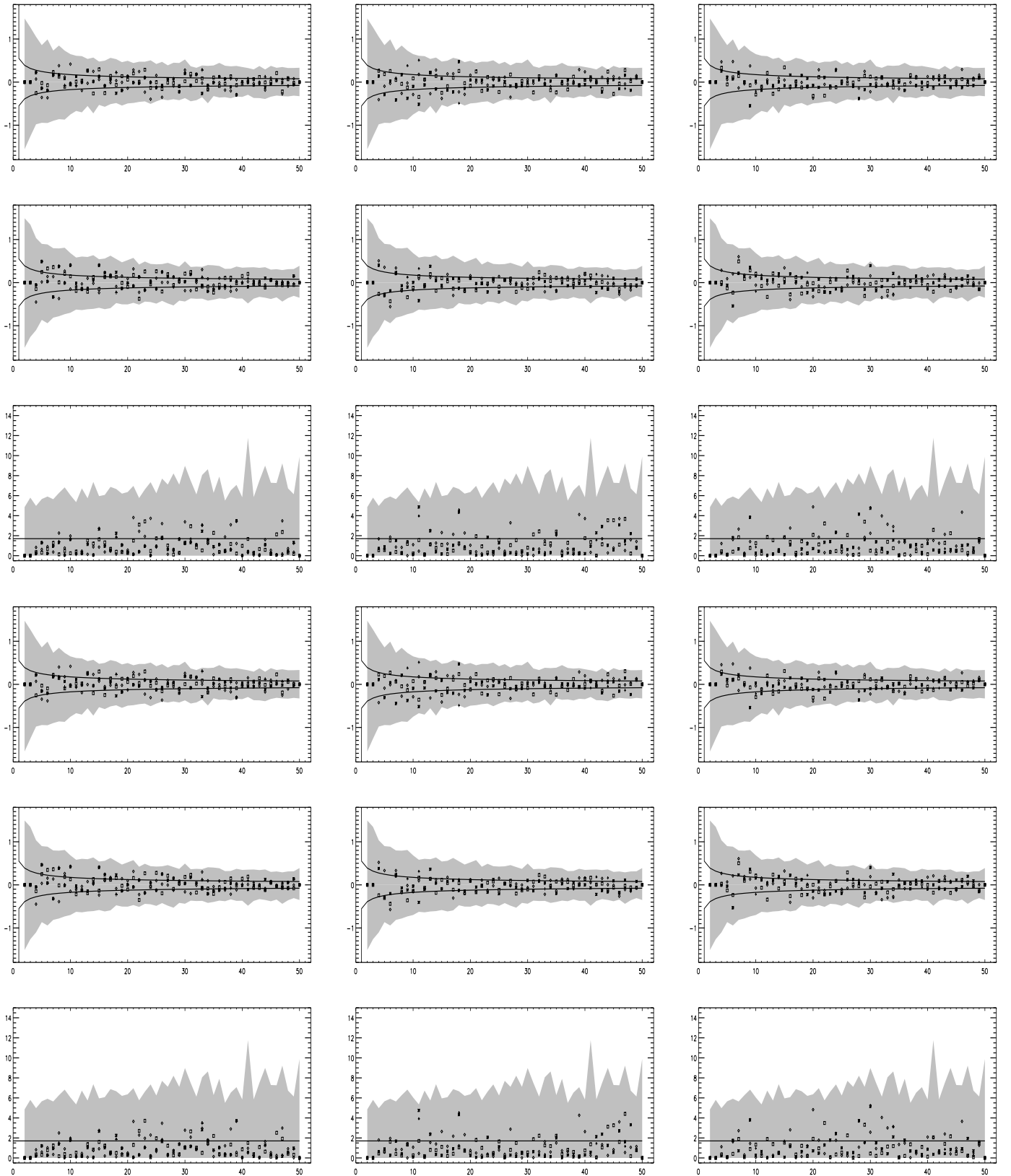


FIG. 13.— The circular statistics for the cross correlation of phases between the TOH FCM and foreground maps (top 3 rows) and between the WFM and foreground maps (lower 3 rows). The notation is the same as Fig.12.

varying component has a characteristic in phases: turning  $\pi/2$  or  $3\pi/2$  from the highly correlated foregrounds.

We further use the standard minimization of the variance to extract the frequency independent signals from all the frequency bands. This component can play a crucial role for the current blind method for component separation in CMB studies. Our method is not only useful for the foreground analysis on the *WMAP* data, it shall be very crucial for the upcoming *Planck* data analysis.

We thank M. Tegmark et al. for providing their processed maps. We thank A. Doroshkevich, M. Demianski and P. R. Christensen for useful discussions. We acknowledge the use of the Legacy Archive for Microwave Background Data Analysis (LAMBDA). Support for LAMBDA is provided by the NASA Office of Space Science. We also acknowledge the use of HEALPIX<sup>6</sup> package (Górski, Hivon & Wandelt 1999) to produce  $a_{\ell m}$  from the *WMAP* data and the use of the GLESP package (Doroshkevich et al. 2003) for data analyses and the whole-sky figures.

#### REFERENCES

- Bardeen, J.M., Bond, J.R., Kaiser, N., Szalay, A.S., 1986, *ApJ*, 304, 15
- Barreiro, R. B., Hobson, M. P., Banday, A. J., Lasenby, A. N., Stolyarov, V., Vielva, P., Górski, K. M., 2003, *MNRAS* submitted (astro-ph/0302091)
- Bennett, C. L., et al., 2003, *ApJ*, 583, 1
- Bennett, C. L., et al., 2003, *ApJS*, 148, 1
- Bennett, C. L., et al., 2003, *ApJS*, 148, 97
- Bond, J. R., Efstathiou, G., 1987, *MNRAS*, 226, 655
- Bouchet, F. R., Gispert, R., 1999, *New Astronomy*, 4, 443
- Chiang, L.-Y., 2001, *MNRAS*, 325, 405
- Chiang, L.-Y., Coles, P., 2000, *MNRAS*, 311, 809
- Chiang, L.-Y., Coles, P., Naselsky, P. D., 2002, *MNRAS*, 337, 488
- Chiang, L.-Y., Naselsky, P. D., Coles, P., 2004, *ApJL*, 602, 1
- Chiang, L.-Y., Naselsky, P. D., Verkhodanov, O. V., Way, M. J., 2003, *ApJL*, 590, 65
- Coles, P., Dineen, P., Earl, J., Wright, D., 2004, *MNRAS* 350 989 (astro-ph/0310252)
- Delabrouille, J., Patanchon, G., Audit, E., 2002, *MNRAS*, 330, 807
- de Oliveira-Costa, A., Tegmark, M., Zaldarriaga, M., Hamilton, A., 2003, *Phys. Rev. D* accepted (astro-ph/0307282)
- Doroshkevich, A. G., Naselsky, P. D., Verkhodanov, O. V., Novikov, D. I., Turchaninov, V. I., Novikov, I. D., Christensen, P. R., 2003, *A&A* submitted (astro-ph/0305537)
- Efstathiou, G., 2003, *MNRAS* submitted (astro-ph/0306431)
- Eriksen, H. K., Hansen, F. K., Banday, A. J., Górski, K. M., Lilje, P. B., 2004, *ApJ* 605 14 (astro-ph/0307507)
- Eriksen, H. K., Banday, A. J., Górski, K. M., Lilje, P. B., 2004, *ApJ* submitted (astro-ph/0403098)
- Finkbeiner, D. P., Davis, M., Schlegel, D. J., 1999, *ApJ*, 524, 867
- Fisher, R., 1993, *Statistical Analysis of Circular Data*, Cambridge University Press, Cambridge
- Górski, K. M., Hivon, E., Wandelt, B. D., 1999, Proceedings of the MPA/ESO Cosmology Conference “Evolution of Large-Scale Structure”, eds. A. J. Banday, R. S. Sheth and L. Da Costa, PrintPartners Ipskamp, NL, ,
- Hansen, F. K., Cabella, P., Marinucci, D., Vittorio, N., 2004, *ApJL* submitted (astro-ph/0402396)
- Hinshaw, G., et al., 2003, *ApJS*, 148, 63
- Hinshaw, G., et al., 2003, *ApJS*, 148, 135
- Hivon, E., Gorski, K. M., Netterfield, C. B., Crill, B. P., Prunet, S., Hansen, F., 2002, *ApJ*, 567, 2
- Hobson, M. P., Jones, A. W., Lasenby, A. N., Bouchet, F. R., 1998, *MNRAS*, 300, 1
- Komatsu, E., et al., 2003, *ApJS*, 148, 119
- Larson, D. L., Wandelt, B. D., 2004, *ApJL* submitted (astro-ph/0404037)
- Martinez-Gonzalez, E., Diego, J. M., Vielva, P., Silk, J., 2003, *MNRAS*, 345, 1101
- Naselsky, P. D., Doroshkevich, A., Verkhodanov, O. V., 2003, *ApJL*, 599, 53
- Naselsky, P. D., Doroshkevich, A., Verkhodanov, O. V., 2004, *MNRAS*, 349, 695
- Naselsky, P. D., Novikov, D. I., Silk, J., 2002, *MNRAS*, 335, 550
- Naselsky, P. D., Verkhodanov, O. V., Chiang, L.-Y., Novikov, I. D., 2003, *ApJ* submitted (astro-ph/0310235)
- Park, C.-G., 2004, *MNRAS*, 349, 313
- Patanchon, G., Snoussi, H., Cardoso, J. F., Delabrouille, J., 2003, PSIP03 conference Grenoble (astro-ph/0302078)
- Stolyarov, V., Hobson, M. P., Ashdown, M. A. J., Lasenby, A. N., 2002, *MNRAS*, 336, 97
- Tegmark, M., Efstathiou, G., 1996, *MNRAS*, 281, 1297
- Tegmark, M., de Oliveira-Costa, A., Hamilton, A., 2003, *Phys. Rev. D*, 68, 123523

<sup>6</sup> <http://www.eso.org/science/healpix/>